Flood mapping using multi-temporal Sentinel-1 SAR images: A case study from Lower Tubarão River Sub-basin, Santa Catarina State, Brazil

Liliana Sayuri Osako [1]

[1] Department of Geology, Federal University of Santa Catarina, Brazil – liliana.osako@ufsc.br

Keywords: Flood areas, SAR imagery, Sentinel-1B, RGB color composite, GEOBIA.

Abstract

Floods are natural hazards triggered by intense rainfall and are particularly destructive in low-lying areas such as floodplains. In flood-prone regions, effective disaster management relies on prevention, monitoring, and emergency response strategies. In this context, remote sensing, especially Synthetic Aperture Radar (SAR), has become indispensable for flood mapping and monitoring due to its ability to acquire data under adverse weather conditions and persistent cloud cover. Multi-temporal SAR imagery processed into RGB composites allows rapid visualization of inundation patterns, while the Geographic Object-Based Image Analysis (GEOBIA) approach improves the classification of flooded areas through the integration of backscatter thresholds and terrain elevation data. This study investigates the spatial and temporal dynamics of flooding in the Lower Tubarão River Sub-basin (LTRSb), southern Brazil, following an extreme precipitation event that produced 260 mm of accumulated rainfall between May 24 and 25, 2019. The Sentinel-1B SAR images, acquired pre- and post-event, were used to map flooded areas with an overall classification accuracy of 88%. The results indicate that three days after the event, flooding covered 140 km² (29%) of the LTRSb, predominantly affecting agricultural (86.3 km²) and pasture areas (47.6 km²). The flooded extent decreased to 62 km² after 15 days and to 15 km² after two months, with agricultural land consistently accounting for 97% of the flooded area. Urbanized areas (≈1 km²) were also impacted, indicating significant risks to infrastructure and public health. These findings highlight the importance of SAR-based flood monitoring for risk assessment and disaster management in hydrographic basins.

1. Introduction

Floods are natural hazards triggered by heavy rainfall events and are characterized by the overflow of rivers. These events frequently occur in regions with tropical and subtropical climates, predominantly affecting low-lying areas, such as coastal plains. In flood-prone regions, it is recommended that disaster management actions be implemented, including prevention, monitoring, and emergency response measures (Calabresi, 1995; Brasil, 2013).

In the context of flood prevention, approaches developed for mapping flooded areas primarily utilize Synthetic Aperture Radar (SAR) imagery, either independently or in combination with optical imagery (Bates et al., 2006; Matgen et al., 2011; Pulvirenti et al., 2011; Schumann and Moller, 2015; Tarpanelli et al., 2022; Alonso-Sarria et al., 2025). SAR is an active remote sensing system capable of artificially generating electromagnetic radiation in the microwave range, with wavelengths varying from 2.4 cm to 100 cm. Due to these unique characteristics, SAR data can be acquired under adverse weather conditions, as electromagnetic radiation within this wavelength range is not affected by cloud cover. Consequently, SAR imagery plays a crucial role in the spatiotemporal mapping of water overflow and recession in river systems following intense precipitation events, particularly in regions that remain cloud-covered.

The generation of RGB color composites from SAR imagery is a widely used and computationally efficient method for enhancing the visualization of flooded areas (ESA, 2017; Ruiz-Ramos et al., 2018; Landuyt et al., 2021). This technique relies on the selection of SAR images acquired at two distinct temporal instances: one prior to the event (reference image) and another following the event (crisis image) associated with heavy rainfall. In the RGB composition, the reference image is assigned to the red channel, while the crisis image is assigned to the green and blue channels. This configuration enables the clear visualization of flooded areas, which appear in shades of red, whereas permanent water bodies are represented in black.

In parallel, various classification methods have been implemented to categorize flooded and non-flooded areas in SAR imagery. Among these approaches, the Geographic Object-Based Image Analysis (GEOBIA) method has gained prominence. This technique is based on image segmentation into homogeneous regions, followed by classification of these regions using multiple attributes — including contextual, textural, and spectral features (Mallinis et al., 2013; Landuyt et al., 2021; Zhang et al., 2021; Alonso-Sarria et al., 2025). Within the set of classification parameters, particular emphasis is placed on backscatter values, expressed in decibels (dB), to define thresholds between flooded and non-flooded areas. Furthermore, the integration of high-resolution Digital Terrain Models (DTMs) enables the generation of contour lines, which assist in estimating minimum flood elevation levels, thereby contributing to a more accurate delineation of potentially affected zones.

In this context, the present study aims to map flood extents using multi-temporal Sentinel-1B SAR imagery acquired before and after the intense precipitation event. Mapping flood-affected areas contributes to a better understanding of surface water dynamics within river basins and supports the development of cartographic products that can aid natural disaster management in flood-prone regions. These products provide vital information for decision-making, resource allocation, and the planning of both preventive and emergency response measures during flood events.

This contribution has been peer-reviewed. The double-blind peer-review was conducted on the basis of the full paper.
https://doi.org/10.5194/isprs-annals-XI-3-2026-441-2026

2. Study area

The study area is in the Lower Tubarão River Sub-basin (LTRSb), which is part of the Tubarão River Basin and covers portions of the municipalities of Tubarão, Laguna, Jaguaruna, Capivari de Baixo, Sangão, and Treze de Maio, in Santa Catarina State, Brazil (Figure 1). The LTRSb covers an area of approximately 1,001 km^2, whose topography is divided into coastal plain (485 km^2, i.e., 48.5%) and mountainous region (515.8 km^2, i.e., 51.5%). The LTRSb (Figure 2) has an extensive area of pasture (52%), and smaller areas of forest and coastal *restinga* areas (16%), agriculture (15%), urbanized area (7.4%), and non-vegetated area, beaches, dunes, rivers, and lagoons (9.6%) (Mapbiomas, 2019).

Between May 24 and 25, 2019, the Santa Marta Lighthouse Meteorological Station (A866), located in Laguna, recorded approximately 260 mm of accumulated precipitation, which led to significant flooding within the LTRSb (Figure 3).

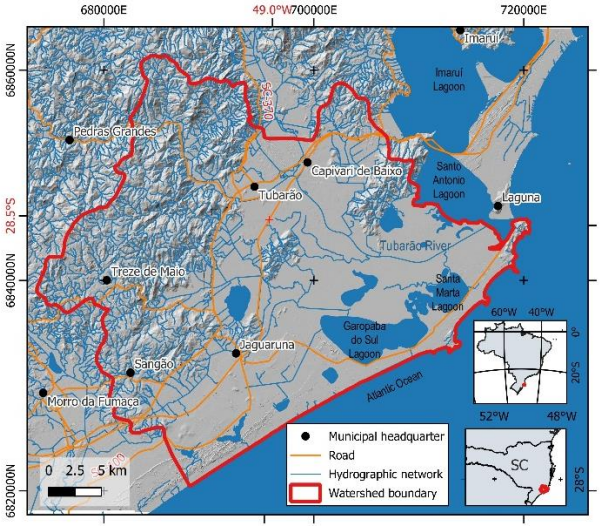

Figure 1. Shaded relief map showing the location of the Lower Tubarão River Sub-basin (LTRSb) in the state of Santa Catarina, Brazil (SDS, 2010).

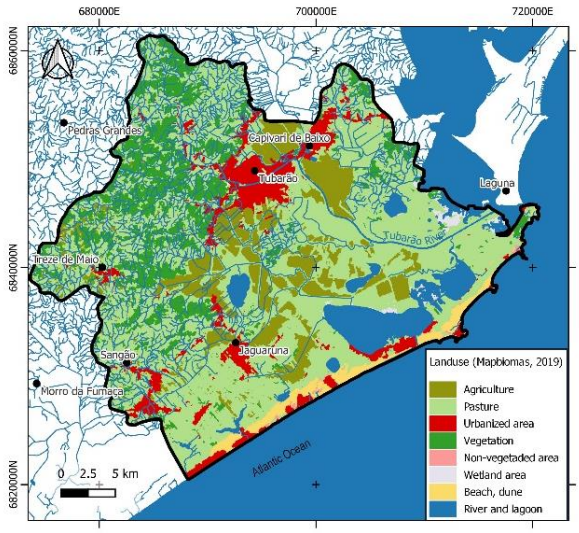

Figure 2. Land use and land cover map of the LTRSb (Mapbiomas, 2019).

3. Materials and methods

For this study, four images from the Sentinel-1 satellite were analyzed. These images were made freely available by the Copernicus Programme (Open Access Hub) of the European Space Agency (ESA), as shown in Figure 2 and Table 1. The images correspond to the Interferometric Wide Swath (IW) acquisition mode, operating in the microwave range, specifically in the C-band, with a frequency between 4 and 8 GHz, an incidence angle ranging from 29° to 46°, and a spatial resolution of 5 m by 20 m. The data are provided at Level 1 Ground Range Detected (GRD) processing level and feature dual polarization: vertical transmit and horizontal receive (VH), as well as vertical transmit and vertical receive (VV).

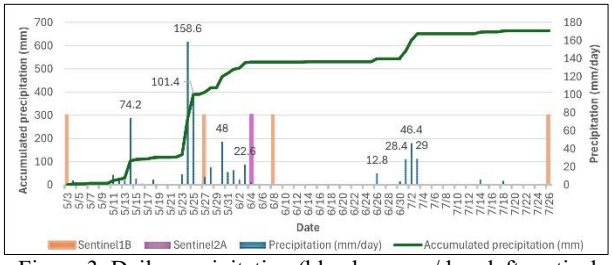

Figure 3. Daily precipitation (blue bar; mm/day; left vertical axis) and daily accumulated precipitation (green line; mm; right vertical axis) over the LTRSb (Fig. 1) from May 02 to July 27 of 2019 (INMET, 2019). The orange bars indicate Sentinel-1B images acquired before and after intense precipitation events in the study area, while the magenta bar indicates a Sentinel-2A image used for validation analysis (ESA, 2024).

3.1 Processing of the SAR data

The digital processing of the SAR images was performed using the Sentinel Application Platform (SNAP), version 8.0.6, developed by SkyWatch and Sensar in partnership with the ESA (ESA, 2024). The Sentinel-1B SAR images were pre-processed through: i) Radiometric calibration: involves converting pixel values into backscatter coefficients and is essential for the quantitative analysis of data across images acquired by the same sensor or by different sensors; ii) Speckle noise removal: SAR images are characterized by a salt-and-pepper texture known as speckle noise, which results from constructive and destructive interference of the returning radar waves. To reduce speckle noise of the Sentinel-1 SAR image, the Lee filter with a 3 × 3 pixel window was applied (Lee and Pottier, 2009); iii) Terrain Correction: Terrain correction corrects geometric distortions induced by the lateral viewing angle of the SAR sensor and by rugged terrain. The terrain correction of the Sentinel-1 SAR images was performed using the Python script *procSentinelRTC_recipe.py*, available in the Sentinel-1 Toolbox (S1TBX) program and SRTM DEM file (ESA, 2024); iv) Linear to decibel conversion: The backscatter coefficient is converted to a logarithmic scale in decibels (dB).

Subsequently, RGB color composites were generated to enhance the flood areas (ESA, 2017). Sentinel-1B SAR images from May 3, 2019 (archive image – A_1), were assigned to the red (R) channel, while images from May 27, 2019 (crisis image – C_1), were assigned to the green (G) and blue (B) channels to generate an RGB color composite (ESA, 2017). This composite ($A_1C_1C_1$) highlighted the flooded areas in the LTRSb immediately following the intense precipitation event. To highlight the dynamics of surface water recession in the LTRSb, two

additional RGB color composites ($A_1C_2C_2$ and $A_1C_3C_3$) were created (Table 1).

3.2 Geographic Object-Based Image Analysis (GEOBIA)

The classification of the Sentinel-1 image was performed in the eCognition software using the GEOBIA method (Udin et al., 2019). A decision tree classifier was adopted to define a sequence of processes for the segmentation and classification of SAR images based on the following parameters (Nussbaum and Menz, 2008; Lang and Blaschke, 2003; Veljanovski et al., 2011): i) Segmentation using a multiresolution segmentation algorithm with shape = 0.1, compactness = 0.5, and scale = 10; ii) Values derived from the SAR image in decibels (dB) to define threshold-based rules for distinguishing between flooded and non-flooded areas (Table 2); iii) Elevation data obtained from a Digital Terrain Model (DTM) were used to establish the maximum elevation of flooded areas and to exclude segments located above this reference altitude (Table 2). The DTM, with a spatial resolution of 1 meter, was derived from an airborne photogrammetric survey funded by the Government of the State of Santa Catarina (SDS, 2010).

Satellite	Date acquired	*Number of days	Image ID	RGB
S-1B	May 03	21 days before	Archive image - A_1	-
	May 27	03 days after	Crisis image - C_1	$A_1C_1C_1$
	June 08	15 days after	Crisis image - C_2	$A_1C_2C_2$
	July 26	63 days after	Crisis image - C_3	$A_1C_3C_3$

Table 1. Selected Sentinel-1B SAR image data for RGB color composites. * Number of days related to the heavy precipitation event of May 24–25, 2019.

Image identification	Backscatter Coefficients (in dB) of the flooded areas	Altitude (in meter) of the flooded area
C_1	-26 < dB < -14	Height less than 10 meters
C_2	-28 < dB < -14	
C_3	-25 < dB < -13	

Table 2. Parameters defined for classification using the GEOBIA approach.

3.3 Data Overlay in a GIS

The analysis of flooded areas in the Lower Tubarão Sub-basin (LTRSb) was conducted in conjunction with ancillary data on key access routes (roads and highways) and land use within a Geographic Information System (GIS) environment (Mapbiomas, 2019). By overlaying these geospatial datasets, cartographic products for the LTRSb were generated.

3.4 Validation

Validation was performed using Sentinel-2A MultiSpectral Instrument (MSI) images with a spatial resolution of 10 m, acquired on June 4, 2019. In the RGB843 color composite, water bodies exhibit spectral and textural characteristics that are distinct from vegetated and urbanized areas. The water bodies exhibit a smooth surface texture with colors varying from light green to black, whereas the vegetated areas display a coarse surface texture with reddish hues, and the urbanized areas present a coarse texture with colors ranging from light green to cyan (Figure 4).

Based on these spectral and textural attributes, 50 validation points were randomly selected within the LTRSb, with a focus on the floodplain areas and their immediate surroundings. Classification accuracy was assessed using a confusion matrix to evaluate the detection of flooded and non-flooded areas derived from Sentinel-1B SAR imagery acquired on May 27, 2019 (C_1).

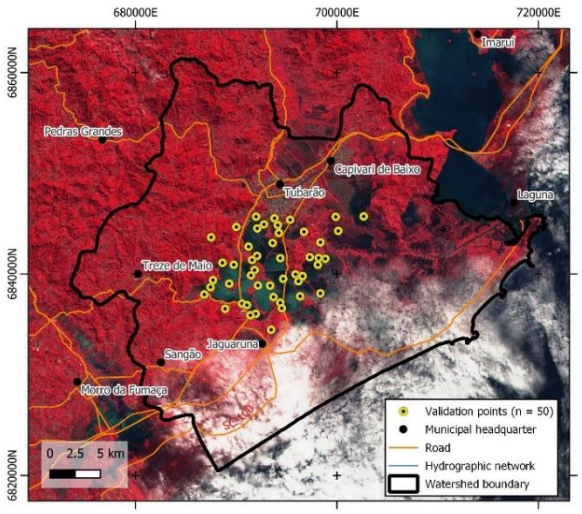

Figure 4. Sentinel-2 RGB843 color composite image acquired on June 4, 2019, showing the locations of validation points (illustrated with yellow-black markers) within the LTRSb.

4. Results and discussion

4.1 SAR Image Analysis

The SAR image from May 3, 2019 (Archive image – A_1), acquired prior to the intense precipitation event in May 2019, highlights water bodies with decibel values ranging from -26 to -14, represented by pixels in black to dark gray. The spatial distribution of these water bodies in the SAR image primarily highlights the Tubarão River, the Imaruí Lagoon, the Santo Antônio Lagoon, the Santa Marta Lagoon, and the Garopaba do Sul Lagoon within the LTRSb (Figure 5A). Target surface roughness controls the intensity of backscatter in Synthetic Aperture Radar (SAR) imagery. Smooth surfaces, such as water bodies, are predominantly characterized by specular reflection, which results in a low radar backscatter signal reaching the sensor. Consequently, Synthetic Aperture Radar (SAR) sensors are widely used for the detection of surface water bodies (Lopes et al., 2023; Alonso-Sarria et al., 2025).

In contrast, light-toned pixels represent non-water surfaces, with backscatter values ranging from −14 dB to 21 dB. These values are associated with arboreal (forest) and herbaceous vegetation (e.g., pastures, coastal restinga, and agricultural fields), as well as urban areas within the LTRSb. According to Bourgeau-Chavez et al. (2009), arboreal and herbaceous vegetation analyzed with C-band sensors exhibit diffuse, double-bounce, and volume scattering mechanisms, which vary according to the degree of flooding. In herbaceous vegetation, under both dry and moist soil conditions with low levels of inundation, diffuse scattering predominates, with some contributions from double-

bounce scattering. Under flooded conditions, with a significant increase in water level over herbaceous areas, a reduction in backscatter occurs due to the predominance of specular reflection at the water surface. Arboreal vegetation typically exhibits volume scattering in C-band sensors due to the presence of branches and leaves in the canopy, which limits electromagnetic radiation penetration to the ground. Consequently, mapping flooded areas in forested environments is more effectively performed using L-band sensor data (longer wavelength), owing to their greater capacity to penetrate the forest canopy (Gašparović et al., 2021).

Buildings and other man-made structures in urban areas are predominantly characterized by double-bounce scattering, particularly for isolated targets observed in high-spatial-resolution SAR imagery. At medium spatial resolutions, however, backscatter is also influenced by additional factors, including the orientation of buildings relative to the satellite flight direction and the width of urban streets (Delgado Blasco et al., 2020).

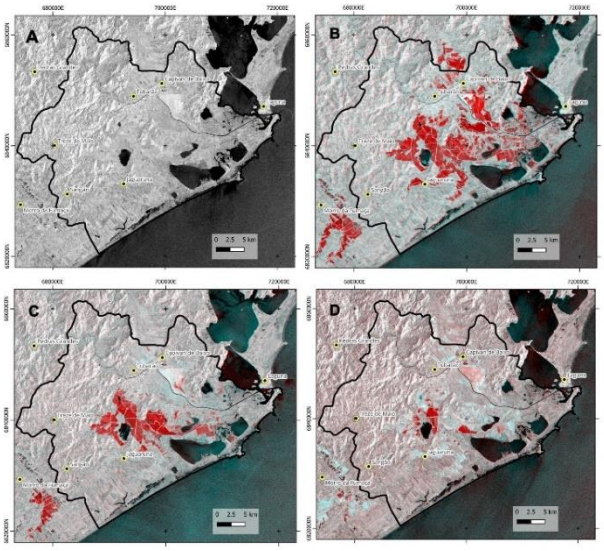

Figure 5. Sentinel-1B images of the LTRSb acquired before and after the intense rainfall event that occurred in May 2019. A) Archive image from May 3, 2019 (A_1); B) Archive and crisis images RGB color composite from May 3 to May 27, 2019 ($A_1C_1C_1$); C) May 3 to June 8, 2019 ($A_1C_2C_2$); and D) May 3 to July 26, 2019 ($A_1C_3C_3$), highlighting the flooded areas in red color.

4.1.1 Inundation Extent: The Sentinel-1B SAR RGB composite ($A_1C_1C_1$) highlights flooded areas in red, covering approximately 140 km² (29%) of the LTRSb coastal plain three days after the heavy precipitation event of May 27, 2019, which recorded 260 mm of accumulated rainfall (Figures 5B and 6, Table 3). Approximately 134 km² (96%) of this flooded area corresponds to land designated for agriculture (86.3 km²) and pasture (47.6 km²), whereas only 1 km² (0.7%) of the urbanized area was affected. The confusion matrix yielded an overall accuracy of 88%, indicating that the proposed methodology reliably detects flooded and non-flooded areas in Sentinel-1B SAR acquired on May 27, 2019 (Table 4).

Fifteen days after the event (June 08, 2019), the RGB composite imagery ($A_1C_2C_2$) shows a reduction in the total flooded area to 62 km² (13%) of the LTRSb coastal plain (Figures 5C and 6, Table 3). Flooded agricultural and pasture lands decreased to 50.2 km² and 10.2 km², respectively, accounting for 97% of the total inundation. Approximately 0.2 km² of the urbanized area remained affected.

Approximately two months after the heavy precipitation event (July 26, 2019), the flooded area ($A_1C_3C_3$) further decreased to 15 km² (3%) of the LTRSb coastal plain (Figures 5D and 6, Table 3). Agricultural and pasture areas represented roughly 14.6 km² (97%) of the total flooded extent. Flooding within urbanized areas was further reduced, totaling only 0.02 km².

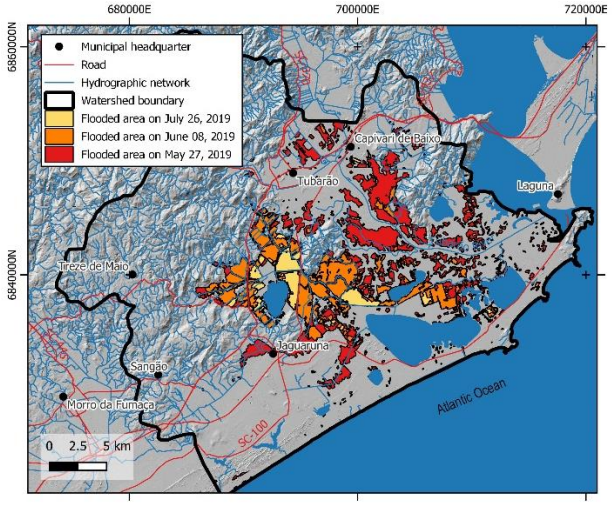

Figure 6. Overlay of flooded areas (polygons) in the LTRSb.

LTRSb with a 485km² coastal plain region			
Land use and land cover	C_1 - 27/05	C_2 - 08/06	C_3 - 26/07
Agriculture	86.3	50.2	11.4
Pasture	47.6	10.2	3.2
Vegetation	0.4	0.03	0.01
Urbanized area	1.0	0.2	0.02
Beach, dunes	3.5	1.4	0.5
River e lagoon	1.2	0.3	0.05
Total flooded area (km²)	140	62	15
Proportion of flooded areas in the coastal plain (%)	29	13	3

Table 3. Flooded area (km²) in the LTRSb from May 27 to July 26, 2019.

	Validation points	
Class outputs	Flooded	Non-flooded
Flooded	46%	4%
Non-flooded	8%	42%
Overall accuracy = 88%		

Table 4. Confusion matrix for flooded area detection in the LTRSb on May 27, 2019 (C_1).

4.1.2 Main area affected by the flooding: The LTRSb floodplain was the area most severely affected by the 2019 flood. In the geological–geomorphological context of the region, this floodplain developed from four Quaternary depositional systems: barrier, coastal plain, lagoonal, and eolian. The flooding mapped in 2019 occurred predominantly within the bay–lagoon sector of the lagoonal depositional system, which serves as the receiving basin for the Tubarão River delta (Giannini, 2002; Giannini et al., 2010).

Over the course of human occupation in this area, the Tubarão River was straightened in response to the region’s recurrent

flooding history. Currently, a dredging project is being implemented to remove sediment from the Tubarão River, with the objective of increasing channel depth and improving its discharge capacity, thereby contributing to flood-mitigation efforts in the LTRSb (Defesa Civil de Santa Catarina, 2025).

The main area affected by the floods was agricultural land. Agricultural activity in the region is predominantly concentrated on rice cultivation, carried out through irrigation systems, which make it one of the main rice producers in the state of Santa Catarina (Epagri, 2019). The floods in the LTRSb occurred at the end of May and persisted until June, coinciding with the off-season period for irrigated rice cultivation, with planting typically occurring between August and November, and harvesting between January and March (Epagri, 2019). It is important to emphasize that the occurrence of extreme precipitation events in the LTRSb during the rice-growing season is likely to have a detrimental impact on rice production. Recent studies have increasingly applied SAR imagery to classify rice growth stages using phenological metrics, facilitating the efficient management of rice production across extensive agricultural areas (Son et al., 2021; Huang et al., 2021; McGiven and Müller, 2025).

Flooding within the urbanized area (approximately 1 km²) demonstrates that the population was directly affected by the extreme precipitation event. The resulting impacts range from loss of property and damage to infrastructure to increased health risks among affected residents.

5. Conclusion

This study highlights the effectiveness of multi-temporal Sentinel-1B SAR imagery for accurately mapping the extent of flooding in the Lower Tubarão River Sub-basin (LTRSb) following the extreme rainfall event of May 2019. RGB color composites derived from SAR imagery, integrated with Geographic Object-Based Image Analysis (GEOBIA) classification, proved highly effective in delineating flooded areas under persistent cloud cover, providing precise information on the spatial extent of inundation resulting from the extreme precipitation. The Sentinel-1 SAR image classification achieved an overall accuracy of 88%.

Immediately following the event, approximately 140 km² (29%) of the LTRSb floodplain was flooded, predominantly affecting agricultural and pasture lands. Urbanized areas (≈1 km²) were also impacted, indicating significant risks to infrastructure and public health. Temporal analysis revealed a rapid recession of floodwaters, with only 3% of the coastal plain remaining submerged two months after the event, reflecting the transient nature of inundation in non-permanent water bodies.

Flood dynamics in the LTRSb are influenced by geomorphological characteristics and anthropogenic interventions. The floodplain, shaped by Quaternary depositional systems, along with the historical straightening of the Tubarão River and ongoing sediment accumulation, contributes to the region’s flood susceptibility. Current dredging projects aim to increase channel depth and discharge capacity, supporting flood mitigation strategies.

The methodology applied in this study provides a robust framework for assessing flood impacts and supporting disaster management. The results offer important and useful information for managing flood risk in the LTRSb and can serve as a model for application in other flood-prone regions.

References

Alonso-Sarria, F., Valdivieso-Ros, C., Molina-Pérez, G., 2025. Detecting flooded areas using Sentinel-1 SAR imagery. *Remote Sens*., 17, 1368. doi.org/ 10.3390/rs17081368.

Bates, P.D., Wilson, M.D., Horritt, M.S., Mason, D.C., Holden, N., Currie, A., 2006. Reach scale floodplain inundation dynamics observed using airborne synthetic aperture radar imagery: Data analysis and modelling. *Journal of Hydrology*, 328: 306-318 (pp.).

Bourgeau-Chavez, L.L., Riordan, K., Powell, R.B., Nicole Miller, N., Nowels, M., 2009. Improving wetland characterization with multi-sensor, multi-temporal SAR and optical/infrared data fusion. *In Advances in Geoscience and Remote Sensing*; Jedlovec, G., Ed.; IntechOpen: London, UK, 2009. doi.org/ 10.5772/8327.

Brasil, 2013. Lei nº 12.608, de 10 de abril de 2012. Institui a Política Nacional de Proteção e Defesa Civil. PNPDEC; dispõe sobre o Sistema de Nacional de Proteção e Defesa Civil - CONPDEC. Diário Oficial da República Federativa do Brasil, Brasília, DF. www.planalto.gov.br/ccivil_03/_ato2011-2014/2012/lei/l12608.htm.

Calabresi, G., 1995. The use of ERS data for flood monitoring: an overall assessment. *In: 2nd ERS Applications Workshop*, December 6-8. ESA, London, UK.

Defesa Civil do Estado de Santa Catarina, 2025. Melhoramento fluvial do Rio Tubarão avança com novos estudos para atualização do projeto. www.defesacivil.sc.gov.br/2025/07/30/melhoramento-fluvial-do-rio-tubarao-avanca-com-novos-estudos-para-atualizacao-do-projeto/.

Delgado Blasco, J.M., Fitrzyk, M., Patruno, J., Ruiz-Armenteros, A.M., Marconcini, M., 2020. Effects on the double bounce detection in urban areas based on SAR polarimetric characteristics. *Remote Sensing*, *12* (7), 1187. doi.org/10.3390/rs12071187.

EPAGRI/CEPA, 2019. Centro de Socioeconomia e Planejamento Agrícola. Síntese Anual da Agricultura de Santa Catarina, 2018-2019. Empresa de Pesquisa Agropecuária e Extensão Rural de Santa Catarina – EPAGRI, 211 p. docweb.epagri.sc.gov.br/website_cepa/publicacoes/Sintese_2018_19.pdf.

ESA, 2024. European Space Agency. www.esa.int/Applications/Observing_the_Earth/Copernicus/Sentinel-1.

ESA, 2017. Hazard: Flood mapping with Sentinel-1. ESA Echoes in Space. www.youtube.com/watch?v=derOXkPCH80.

Gašparovi´c, M., Klobu˘car, D., 2021. Mapping floods in lowland forest using Sentinel-1 and Sentinel-2 data and an object-based approach. *Forests*, 12, 553. doi.org/ 10.3390/f1205055.

Giannini, P.C.F., 2002. Complexo lagunar centro-sul catarinense – valioso patrimônio sedimentológico, arqueológico e histórico. In: Schobbenhaus, C., Campos, D.A., Queiroz, E.T.; Winge, M.; Berbert-Born, M. (Eds.). *Sítios geológicos e Paleontológicos do Brasil*. Brasília: DNPM, 2002. p. 213-222. https://sigep.eco.br/sitio075/sitio075.pdf.

Giannini, P.C.F., Villagran, X.S., Fornari, M., Nascimento Junior, D.R., Menezes, P.M.L., Tanaka, A.P.B., Assunção, D.C., DeBlasis, P., Amaral, P.G.C., 2010. Interactions between sedimentary evolution and prehistoric human occupation in the south-central coast of Santa Catarina, Brazil. *Bol. Mus. Para. Emílio Goeldi*, Belém, vol.5, no.1, p. 105-128. doi.org/10.1590/S1981-81222010000100008.

Huang, X., Runkle, B.R.K., Isbell, M., Moreno-García, B., McNairn, H., Reba, M.L., & Torbick, N., 2021. Rice inundation assessment using polarimetric UAVSAR data. *Earth and Space Science*, 8, e2020EA001554. doi.org/10.1029/2020EA001554.

INMET, 2019. Instituto Nacional de Meteorologia. https://portal.inmet.gov.br/.

Landuyt, L., Van Coillie, F.M.B., Vogels, B., Dewelde, J., Verhoest, N.E.C., 2021. Towards operational flood monitoring in Flanders using Sentinel-1. *IEEE Journal Selected Topics in Applied Earth Observation and Remote Sensing*, v. 14., p. 1104-11018. doi.org/10.1109/JSTARS.2021.3121992.

Lang, S., Blaschke, T., 2003. Hierarchical object representation. Comparative multiscale mapping of anthropogenic and natural features. *International Archives of Photogrammetry, Remote Sensing and Spatial Information Sciences* 34 (Part 3/W8), 181–186. www.isprs.org/proceedings/xxxiv/3-W8/papers/pia03_s8p1.pdf

Lee, J. S., Pottier, E. 2009. *Polarimetric SAR Radar Imaging: From Basic to Applications*, CRC Press, Taylor & Francis Group.

Lopes, I.A.M., Carvalho Junior, O.A., Sano, E.E., 2023. Delimitation of flooded areas based on Sentinel-1 SAR data processed through machine learning: A study case from Central Amazon, Brazil. *Finisterra*, LVIII(123), 2023, pp. 87-109. doi.org/10.18055/Finis30884.

Mallinis, G., Gitas, I.Z., Giannakopoulos, V., Maris, F., Tsakiri-Strati, M., 2013. An object-based approach for flood area delineation in a transboundary area using ENVISAT ASAR and LANDSAT TM data, *International Journal of Digital Earth*, 6: sup2, 124-136, doi.org/10.1080/17538947.2011.641601.

Mapbiomas, 2019. Projeto MapBiomas – Coleção 10 da Série Anual de mapas de cobertura e uso da terra do Brasil. https://plataforma.brasil.mapbiomas.org/coverage/.

Matgen, P., Hostache, R., Schumann, G., Pfister, L., Hoffmann, L., Savenije, H.H.G., 2011. Towards an automated SAR-based flood monitoring system: Lessons learned from two case studies. *Physics and Chemistry of the Earth*, 36: 241–252 (pp.), 2011. doi.org/10.1016/j.pce.2010.12.009.

McGiven, L.E., Müller, M.F., 2025. Unsupervised mapping of rice paddy fields and their inundation patterns using Sentinel-1 SAR images and GIS, *European Journal of Remote Sensing*, 58:1, 2484711, doi.org/10.1080/22797254.2025.2484711.

Nussbaum, S., Menz, G., 2008. Object-based analysis of iranian nuclear facilities. *In: Object-based Image Analysis and Treaty Verification*. Springer, Dordrecht. doi.org/10.1007/978-1-4020-6961-1_7.

Pulvirenti, L., Chini, M., Pierdicca, N., Guerriero, L., Ferrazzoli. P., 2011. Flood monitoring using multi-temporal COSMO-SkyMed data: Image segmentation and signature interpretation. *Remote Sensing of Environment*, 115: 990-1002 (pp.). doi.org/10.1016/j.rse.2010.12.002.

Ruiz-Ramos, J., Marino, A., Boardman, C.P., 2018. Using Sentinel-1 SAR form monitoring long term variation in burnt forest areas. *IGARSS 2018-2018 IEEE International Geoscience and Remote Sensing*. doi.org/10.1109/IGARSS.2018.8518960.

Schumann, G.J.P., Moller, D. K., 2015. Microwave remote sensing of flood inundation. *Physics and Chemistry of the Earth*, Parts A/B/C, vol. 83–84, p. 84-95. doi.org/10.1016/j.pce.2015.05.002.

SDS - Secretaria de Estado do Desenvolvimento Econômico Sustentável, 2010. Download of orthophotos, Digital Surface Model and Digital Elevation Model. sigsc.sds.sc.gov.br. (5 January 2020).

Son, N.T., Chen, C.F., Chen, C.R., Toscano, P., Cheng, Y.S., Guo, H.Y., Syu, C. H., 2021. A phenological object-based approach for rice crop classification using time-series Sentinel-1 Synthetic Aperture Radar (SAR) data in Taiwan. *International Journal of Remote Sensing*, *42* (7), 2722–2739. doi.org/10.1080/01431161.2020.1862440.

Tarpanelli, A., Mondini, A.C., Camici. S., 2022. Effectiveness of Sentinel-1 and Sentinel-2 for flood detection assessment in Europe. *Natural Hazards and Earth System Sciences*, 22, 2473–2489. doi.org/10.5194/nhess-22-2473-2022.

Udin, K., Matin, M.A., Meyer, F.J., 2019. Operational flood mapping using multi-temporal Sentinel-1 SAR images: A case study from Bangladesh. *Remote Sensing*, 11 (13), 1581. doi.org/10.3390/rs11131581.

Veljanovski, T., Kanjir, U., Ostir, K., 2011. Object-based image analysis of remote sensing data. *Geodetski Vestnik*, vol. 55, no. 4, pp. 678-688, 2011. doi.org/10.15292/geodetski-vestnik.2011.04.641-664.

Zhang, X., Chan, N.W.C., Pan, B., Ge, X., Yang, H., 2021. Mapping flood by the object-based method using backscattering coefficient and interference coherence of Sentinel-1 time series. *Science of the Total Environment*. 794. doi.org/10.1016/j.scitotenv.2021.148388.